Three-Dimensional Neutronics Analysis for the LIBRA-SP Light Ion Fusion Power Reactor

M.E. Sawan

June 1998

UWFDM-1076

Presented at the 13th Topical Meeting on the Technology of Fusion Energy, June 7–11, 1998, Nashville TN

FUSION TECHNOLOGY INSTITUTE

UNIVERSITY OF WISCONSIN

MADISON WISCONSIN

THREE-DIMENSIONAL NEUTRONICS ANALYSIS FOR THE LIBRA-SP LIGHT ION FUSION POWER REACTOR

M.E. Sawan
University of Wisconsin-Madison, Fusion Technology Institute
1500 Engineering Drive
Madison, Wisconsin 53706, USA
(608) 263-5093

ABSTRACT

Three-dimensional (3-D) neutron-gamma transport calculations have been performed for the LIBRA-SP chamber with detailed geometrical modeling and results were compared to results based on one-dimensional (1-D) calculations. The overall tritium breeding ratio is 1.396. This is only 3% lower than the value predicted from the 1-D results. The overall reactor energy multiplication is 1.157 which is only 2% lower than the value estimated from the 1-D calculations. Larger differences were observed in the local heating and damage results obtained from the 1-D and 3-D calculations.

I. INTRODUCTION

LIBRA-SP is a 1000 MW_e light ion beam power reactor design study which utilizes a self-pinched mode for propagating the ions from the ion-diode to the target[1]. The reactor is driven by 7.8 MJ of 30 MeV Li ions at a repetition rate of 4.2 Hz and a target yield of 552 MJ. A schematic of the LIBRA-SP target chamber is shown in Fig. 1. Rigid ferritic steel tubes called PERIT (perforated rigid tubes) units are used for chamber wall protection. These tubes are equipped with tiny nozzles that spray vertical fans of liquid metal, overlapping each other such that the front two rows of tubes are completely shadowed from the target emanations. The PERIT units are followed by a 50 cm thick steel reflector which is also the vacuum boundary. The whole chamber is surrounded by a steel reinforced concrete shield.

Neutronics analysis has been performed previously for the LIBRA-SP chamber using 1-D spherical geometry calculations for the different regions surrounding the target[2]. The 1-D local nuclear parameters were combined with the coverage fractions for the reactor regions to determine the overall tritium breeding ratio (TBR) and energy multiplication. It has been demonstrated previously[3] that in the preliminary stages of the design, this approach yields reasonable estimates for the overall nuclear parameters that are not much different from the 3-D results. However, the differences are expected to be larger for the local damage and heating results due to the impact of the different materials used in the chamber regions on the secondary neutrons and gamma photons contributing to damage and heating in other regions. In addition, the geometrical configuration of the front surface of each region relative to the target in the actual geometry results in an angular distribution of incident neutrons which is different from that in the 1-D spherical geometry leading to different damage and heating profiles[4]. In this paper, a 3-D neutronics analysis for the LIBRA-SP chamber is presented and the results are compared to the results from the previous 1-D calculations.

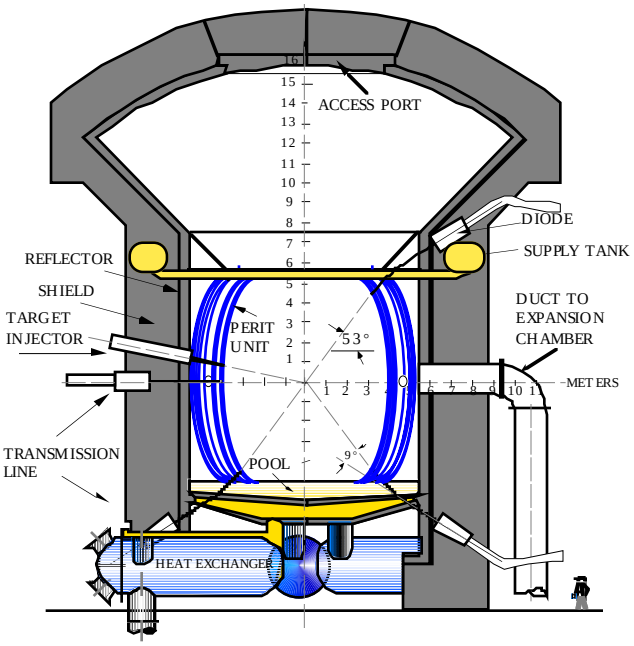

Fig. 1. Cross-sectional view of LIBRA-SP

II. 3-D CALCULATIONAL MODEL

The continuous energy, coupled neutron-gamma-ray Monte Carlo code MCNP-4A[5] has been used with nuclear data based on the international fusion evaluated nuclear

data library FENDL-1[6]. In the previous 1-D calculations[2], multi-group cross section data based on the ENDF/B-VI evaluation was used. The detailed geometrical configuration of the chamber has been modeled for the 3-D neutronics calculations. The model includes the 120 cm thick PERIT tube region with 0.5 packing fraction. The tubes are made of the ferritic steel alloy HT-9 and consist of 8% HT-9 and 92% $Li_{17}Pb_{83}$. The $Li_{17}Pb_{83}$ eutectic is enriched to 90% ^{6}Li. A $Li_{17}Pb_{83}$ supply ring is also modeled at the top of the PERIT region. In the bottom region, the 60 cm deep $Li_{17}Pb_{83}$ pool followed by a 25 cm perforated plate consisting of 80% HT-9 and 20% $Li_{17}Pb_{83}$ and a 50 cm deep sump tank of $Li_{17}Pb_{83}$, are modeled. A region representative of the intermediate heat exchanger (IHX) is also included. The 50 cm thick chamber wall consisting of 90% HT-9 and 10% $Li_{17}Pb_{83}$ is modeled with its vertical cylindrical part and the mushroom shaped roof. The chamber is surrounded by a concrete biological shield that consists of 70% concrete, 20% carbon steel C1020 and 10% He coolant. The biological shield thickness is 2.5 m on the side and 2.6 m at the top. The output of the MCNP geometry plotting routine given in Fig. 2 shows a vertical cross section of the 3-D geometrical model. Surface flux tallies were used to determine the peak radiation effects at the front surfaces of the chamber components and cell flux and energy deposition tallies were used to determine the average nuclear parameters in the different regions. The penetrations for ion beams and target injection are not included in the model. Only 0.004% of the source neutrons stream directly into these penetrations resulting in a negligible effect on the chamber nuclear parameters.

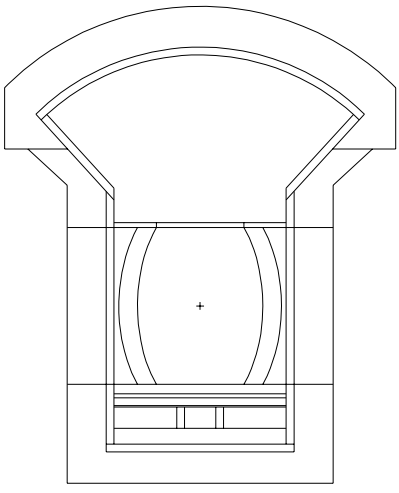

Fig. 2. Three-dimensional neutronics model for the LIBRA-SP chamber.

A point source was used in the center of the chamber emitting neutrons and gamma photons with the LIBRA-SP target spectrum. The source spectrum used in the 1-D calculations[2] was obtained from target neutronics which uses a single target configuration at ignition with uniform densities and source. The detailed results of the hydrodynamics calculations were utilized to perform new target neutronics calculations that take into account the varying configuration during the burn as well as the distributed material densities and fusion neutron source profile[7]. The target spectrum resulting from these calculations is used for sampling the energy of source neutrons and gamma photons in the 3-D calculation. 1.042 neutrons are emitted from the target for each DT fusion reaction with an average energy of 11.8 MeV. For each DT fusion reaction, 0.0033 gamma photons are emitted from the target with an average energy of 3.66 MeV.

The geometry splitting with Russian Roulette variance reduction techniques were utilized in the MCNP calculation to improve the statistical accuracy of the nuclear responses. Two separate calculations were performed and the nuclear response results were added. The first one is a coupled neutron-gamma calculation with a neutron source corresponding to the spectrum of neutrons emitted from the target. The second calculation is a gamma transport calculation with the spectrum of gamma photons emitted from the target as a source. The weight of the source particle was modified to 1.042 and 0.0033 in the neutron and gamma calculations, respectively, to yield results per DT fusion. The damage and heating responses were normalized to a DT fusion power of 2318 MW that corresponds to 8.22×10^{20} DT fusion/s. The two calculations have been performed using 10,000 source particles in each yielding statistical uncertainties <0.5% in the calculated overall neutronics parameters and <5% is the local damage and heating results.

III. TRITIUM BREEDING AND NUCLEAR HEATING

Table 1 gives the tritium production and nuclear heating results in the different chamber regions. About 72% of the total tritium breeding is contributed by the $Li_{17}Pb_{83}$ in the PERIT tubes. The tritium bred in the $Li_{17}Pb_{83}$ coolant of the chamber wall amounts to 13% of the total tritium production. A large fraction of this (64%) is contributed by the unprotected chamber roof. The overall tritium breeding ratio is 1.396. This is only 3% lower than the value predicted from coupling the 1-D results with coverage fractions of the different chamber regions[2]. The nuclear energy deposition in the PERIT units amounts to 72% of the total nuclear energy. The chamber wall contributes 18% of the total nuclear heating. The total energy deposited by neutrons and gamma

Table 1. Tritium Production and Nuclear Heating in the LLIBRA-SP Chamber

Region	Tritium Breeding (Tritons/Fusion)	Nuclear Heating (MeV/Fusion)
Blanket Region		
$Li_{17}Pb_{83}$ Supply	0.051	0.361
PERIT Units	1.004	10.998
Total	1.055	11.359
Bottom Region		
Bottom Pool	0.148	1.262
Perforated Plate	0.004	0.042
Sump	0.006	0.029
IHX	0.0002	0.001
Total	0.158	1.334
Chamber Wall		
Vertical Side Wall		
Behind PERIT Units	0.054	0.661
Above PERIT Units	0.010	0.130
Below PERIT Units	0.001	0.010
Roof	0.067	1.294
Top	0.050	0.646
Side	0.183	2.741
Total		
Chamber Total	1.396	15.434

photons in LIBRA-SP is 15.434 MeV per DT fusion. Since the energy carried by neutrons and gamma photons emitted from the target and incident on the chamber components is 12.3 MeV per fusion, the nuclear energy multiplication, M_n, of the chamber is 1.255.

To take into account the surface energy deposited by x-rays and ion debris and the energy lost by endoergic reactions in the target, an overall reactor energy multiplication, M_o, is defined as the ratio of the total power deposited to the DT fusion power. Since the target neutronics indicate that 69.89% of the fusion power is carried by neutrons and gamma photons and 28% is carried by x-rays and ion debris, the overall reactor energy multiplication is 1.157. This value is only 2% lower than the value estimated from the 1-D calculations[2]. The very small difference between the 3-D results for overall tritium breeding and energy multiplication and the 1-D estimates demonstrates that coupling the simple 1-D results with the appropriate coverage fractions provides a very useful tool for predicting the overall nuclear parameters for fusion systems in the early stage of the design where several design iterations are needed.

Table 2 gives the power deposited by neutrons and gamma photons in the different regions of the LIBRA-SP chamber. The total power deposited volumetrically in the chamber is 2032.3 MW. Adding the 649 MW deposited at the front surfaces by x-rays and ion debris, the total thermal power in the LIBRA-SP chamber is 2681.3 MW. The largest power density is 9.15 W/cm^3 in the PERIT tubes because of their proximity to the target. The total power deposited in the biological shield is only 66 MW with 70% of it contributed by the shield behind the unprotected roof. This is removed by the helium coolant and is not included in the power cycle.

IV. RADIATION DAMAGE AND GAS PRODUCTION IN STRUCTURAL MATERIAL

The peak atomic displacement and helium production rates in the HT-9 structure have been determined using surface flux tallies. The results are shown in Table 3. In this study, we adopted a conservative end-of-life dpa limit of 150 dpa for the ferritic steel HT-9. The peak dpa rate in the PERIT tubes is 67.1 dpa/FPY implying a lifetime of 2.2 FPY. It is interesting to note that the peak dpa rate in the PERIT tubes obtained from the 3-D calculation is about 30% lower than the 1-D prediction[2]. This is attributed to the fact that in the 1-D calculation, the target is fully surrounded by the material composition corresponding to the PERIT units while in the actual 3-D geometry, less secondary neutrons will end up back in the chamber because of the mushroom shaped configuration and due to the lower neutron multiplication in the mostly steel roof. On the other hand, the peak He production,

which has a higher threshold energy, is slightly larger (2%) than the 1-D estimate because of the harder spectrum of secondary neutrons scattered from the roof compared to the lead rich material used in the 1-D model.

Table 2. Power Deposited in the LIBRA-SP Chamber

Region	Power (MW)
Blanket Region	
$Li_{17}Pb_{83}$ Supply	47.57
PERIT Units	1448.21
Total	1495.78
Bottom Region	
Bottom Pool	166.16
Perforated Plate	5.52
Sump	3.87
IHX	0.13
Total	175.68
Chamber Wall	
Vertical Side Wall	
Behind PERIT Units	87.03
Above PERIT Units	17.07
Below PERIT Units	1.35
Roof	
Top	170.34
Side	85.05
Total	360.84
Chamber Total	2032.30

The peak dpa and He production rates in the chamber wall behind the PERIT tubes are 2.43 dpa/FPY and 0.99 appm/FPY, respectively. For the same reasons discussed above, these values are lower by 42% for dpa and higher by 7% for He production compared to the values predicted from the 1-D calculations. For 30 FPY of operation, the end-of-life peak dpa in the side chamber wall is only 73 dpa and easily qualifies as a lifetime component with a comfortable margin of 2. The part of the chamber wall below the PERIT tubes experiences the least damage and He production rates because of the significant attenuation and neutron slowing down provided by the $Li_{17}Pb_{83}$ in the bottom region. While the He/dpa ratio is 6.64 at the front of the PERIT tubes exposed to direct source neutrons, it drops to 0.41 at the chamber wall behind the PERIT tubes and only 7.6×10^{-5} in the part of the chamber wall below the PERIT tubes because of the significant spectrum softening by the lead in the $Li_{17}Pb_{83}$ in the bottom pool.

The peak dpa rate in the bottom perforated plate implies an end-of-life dpa of only 33 dpa. It easily qualifies as a lifetime component with a large margin. It is interesting to note that the 3-D results for the dpa and He production rates in the perforated plate behind the $Li_{17}Pb_{83}$ pool are lower than the 1-D predictions by factors of 4 and 2, respectively. This is due to lower secondary neutron production from the steel in the roof and PERIT tubes in the actual 3-D geometry compared to the 1-D model where the target is fully surrounded by $Li_{17}Pb_{83}$ which leads to significant neutron multiplication. The effect is less pronounced for He production because of the harder spectrum in the 3-D calculation. The geometrical configuration of the roof indicates that the side wall is completely shadowed from the direct source neutrons. As a result, only secondary neutrons scattered back from the top dome of the roof contribute to damage in the side of the roof. This is clearly demonstrated by the results in Table 3. The peak dpa rate in the side is 33% lower than that in the top dome of the roof. The effect is more pronounced for He production, produced by higher energy neutrons, where a factor of 15 lower values are obtained in the side of the roof. The peak end-of-life dpa in the roof is 103 dpa implying that it is a lifetime component.

Table 3. Peak Radiation Damage and Gas Production Rates in HT-9 Structure

Region	Peak Atomic Displacement Rate (dpa/FPY)	Peak Helium Production Rate (appm/FPY)
PERIT Units	67.090	445.76
Vertical Side Wall		
Behind PERIT Units	2.430	0.99
Above PERIT Units	2.330	0.86
Below PERIT Units	0.074	5.62×10^{-6}
Perforated Plate Behind Pool	1.108	0.53
Roof		
Top	3.446	18.80
Side	2.295	1.27

V. SUMMARY AND CONCLUSIONS

Three-dimensional neutron-gamma transport calculations have been performed for the LIBRA-SP chamber using the continuous energy, coupled neutron-gamma-ray Monte Carlo code MCNP-4A with the FENDL-1 cross section data. The detailed geometrical configuration of the chamber has been modeled for the 3-D neutronics calculations. A point source was used in the center of the chamber emitting neutrons and gamma photons with the LIBRA-SP target spectrum that takes into account the varying configuration during the burn as well as the distributed material densities and fusion neutron source profile. The overall tritium breeding ratio is 1.396 and the overall reactor energy multiplication is 1.157. Calculated damage rates in the chamber wall, roof, and bottom perforated plate imply that these components will last for the whole reactor lifetime. On the other hand, the PERIT tubes will require several replacements with the front row having a lifetime of 2.2 FPY.

The 3-D results were compared to those obtained from the previous 1-D spherical geometry calculations for the different regions surrounding the target. It is concluded that combining the 1-D results with the coverage fractions for the reactor regions to determine the overall tritium breeding ratio and energy multiplication leads to values that are within 3% of those obtained from the detailed 3-D calculations. However, larger differences were observed in the local heating and damage results. These are attributed to the geometrical configuration and the impact of the different materials used in the chamber regions on the secondary neutrons and gamma photons.

ACKNOWLEDGMENT

Support for this work was provided by the U.S. Department of Energy through Sandia National Laboratory and Forschungszentrum Karlsruhe.

REFERENCES

1. B. Badger, et al., "LIBRA-SP - A Light Ion Fusion Power Reactor Design Study Utilizing a Self-Pinched Mode of Ion Propagation," University of Wisconsin Fusion Technology Institute Report UWFDM-982, June 1995.

2. M. Sawan, "Nuclear Analysis for the Light Ion Fusion Power Reactor LIBRA-SP," Fusion Technology, 30, 1579 (1996).

3. M. Sawan et al., "Three-Dimensional Neutronics Analysis of the U.S. Blanket Design for ITER," Fusion Technology 19, 1513 (1991).

4. M. Sawan, "Geometrical, Spectral and Temporal Differences between ICF and MCF Reactors and Their Impact on Blanket Nuclear Parameters," Fusion Technology 10/3, 1483 (1986).

5. J. Briesmeister, Ed., "MCNP, A General Monte Carlo N-Particle Transport Code, Version 4A," LA-12625-M (1993).

6. R. MacFarlane, "FENDL/MC-1.0, Library of Continuous Energy Cross Sections in ACE Format for MCNP-4A," Summary Documentation by A. Pashchenko, H. Wienke and S. Ganesan, Report IAEA-NDS-169, Rev. 3, International Atomic Energy Agency (Nov. 1995).

7. J. MacFarlane, M. Sawan, G. Moses, P. Wang, and R. Olson, "Numerical Simulation of the Explosion Dynamics and Energy Release from High-Gain ICF Targets," Fusion Technology, 30, 1569 (1996).